Slow-binding inhibition of acetylcholinesterase by an alkylammonium derivative of 6-methyluracil: mechanism and possible advantages for myasthenia gravis treatment

Alexandra D. Kharlamova*[1], Sofya V. Lushchekina†[1], Konstantin A. Petrov*, Ekaterina D. Kots†, Florian Nachon‡, Marielle Villard-Wandhammer‡, Irina V. Zueva*, Eric Krejci§, Vladimir S. Reznik*, Vladimir V. Zobov*, Evgeny E. Nikolsky||¶ and Patrick Masson¶[2]

*A.E. Arbuzov Institute of Organic and Physical Chemistry of Russian Academy of Sciences, Arbuzov Str. 8, Kazan 420088 Russia
†N.M. Emanuel Institute of Biochemical Physics of Russian Academy of Sciences, Moscow 119334, Russia
‡Institut de Recherche Biomédicale des Armées, 91223 Brétigny-sur-Orge, France
§COGNition ACtion Group, CNRS, Université Paris Descartes 75006 Paris, France
||Kazan Institute of Biochemistry and Biophysics of Russian Academy of Sciences, P.O. Box 30, Kazan 420111, Russia
¶Kazan Federal University, Neuropharmacology Lab., Kremlevskaia St. 18, Kazan 420000, Russia

Inhibition of human AChE (acetylcholinesterase) and BChE (butyrylcholinesterase) by an alkylammonium derivative of 6-methyluracil, C-547, a potential drug for the treatment of MG (myasthenia gravis) was studied. Kinetic analysis of AChE inhibition showed that C-547 is a slow-binding inhibitor of type B, i.e. after formation of the initial enzyme·inhibitor complex ($K_i = 140$ pM), an induced-fit step allows establishment of the final complex ($K_i^* = 22$ pM). The estimated k_{off} is low, 0.05 min^{-1}. On the other hand, reversible inhibition of human BChE is a fast-binding process of mixed-type ($K_i = 1.77$ μM; $K_i' = 3.17$ μM). The crystal structure of mouse AChE complexed with C-547 was solved at 3.13 Å resolution. The complex is stabilized by cation–π, stacking and hydrogen-bonding interactions. Molecular dynamics simulations of the binding/dissociation processes of C-547 and C-35 (a non-charged analogue) to mouse and human AChEs were performed. Molecular modelling on mouse and human AChE showed that the slow step results from an enzyme conformational change that allows C-547 to cross the bottleneck in the active-site gorge, followed by formation of tight complex, as observed in the crystal structure. In contrast, the related non-charged compound C-35 is not a slow-binding inhibitor. It does not cross the bottleneck because it is not sensitive to the electrostatic driving force to reach the bottom of the gorge. Thus C-547 is one of the most potent and selective reversible inhibitors of AChE with a long residence time, $\tau = 20$ min, longer than for other reversible inhibitors used in the treatment of MG. This makes C-547 a promising drug for the treatment of this disease.

Key words: acetylcholinesterase, butyrylcholinesterase, 6-methyluracil, molecular modelling, slow-binding inhibition, X-ray structure.

INTRODUCTION

MG (myasthenia gravis) is a chronic autoimmune neuromuscular disorder characterized by fluctuating weakness of voluntary skeletal muscles. Weakness in MG is caused by autoantibodies directed against muscle-type nAChRs (nicotinic acetylcholine receptors) $(\alpha 1)2\beta 1\delta\varepsilon$. Antibodies reduce the number of receptors at neuromuscular junctions [1,2]. The cause of the autoimmune response is unknown [3], thus only symptomatic therapies are available. For pharmacological correction of synaptic failure in MG, drugs used are reversible inhibitors of AChE (acetylcholinesterase) and BChE (butyrylcholinesterase). Both enzymes catalyse the hydrolysis of ACh (acetylcholine), thus terminating its action at neuromuscular junctions [4]. Other treatments of MG include immunosuppressive drugs and, in some cases, thymectomy [5].

AChE inhibition in symptomatic treatment of MG extends the effects of ACh. Extension of the ACh lifetime in the synaptic cleft, where receptors affected by autoantibodies are localized, leads to repetitive activation of nAChRs. This compensates for the reduction in nAChR density and, as a consequence, rescues muscle contractions. Inhibition of BChE, localized on the surface of terminal Schwann cells [6], has no effect on lifetime of ACh in the synaptic cleft, but activates the loop of negative autoregulation of ACh release via α_7 nAChRs localized on terminal Schwann cells. Therefore AChE inhibition increases the lifetime of ACh molecules in the synaptic cleft, while BChE inhibition triggers reduction of the number of ACh molecules released in the synaptic cleft. When a selective AChE inhibitor is used to increase the ACh concentration in the synaptic cleft of myasthenic rats, the functional improvement is better than with a non-selective inhibitor of ChEs (cholinesterases), during which inhibition of BChE counteracts the positive action of AChE inhibition [7].

Currently, the most frequently used ChE inhibitor in treatment of muscle weakness symptoms in MG patients is pyridostigmine. This pseudo-reversible carbamylating agent does not cross the blood–brain barrier. Although its selectivity for human (h) AChE is poor [K_i ratio (BChE/AChE) ≈ 6] [8], its residence on

Abbreviations: ACh, acetylcholine; AChE, acetylcholinesterase; BChE, butyrylcholinesterase; ChE, cholinesterase; h, human; LGA, Lamarckian Genetic Algorithm; LS, local search; MG, myasthenia gravis; m, mouse; nAChR, nicotinic acetylcholine receptor; PAS, peripheral anionic site; SMD, steered molecular dynamics; TAA, tetra-alkylammonium.

[1] These authors contributed equally to this work.

[2] To whom correspondence should be addressed (email pym.masson@free.fr).

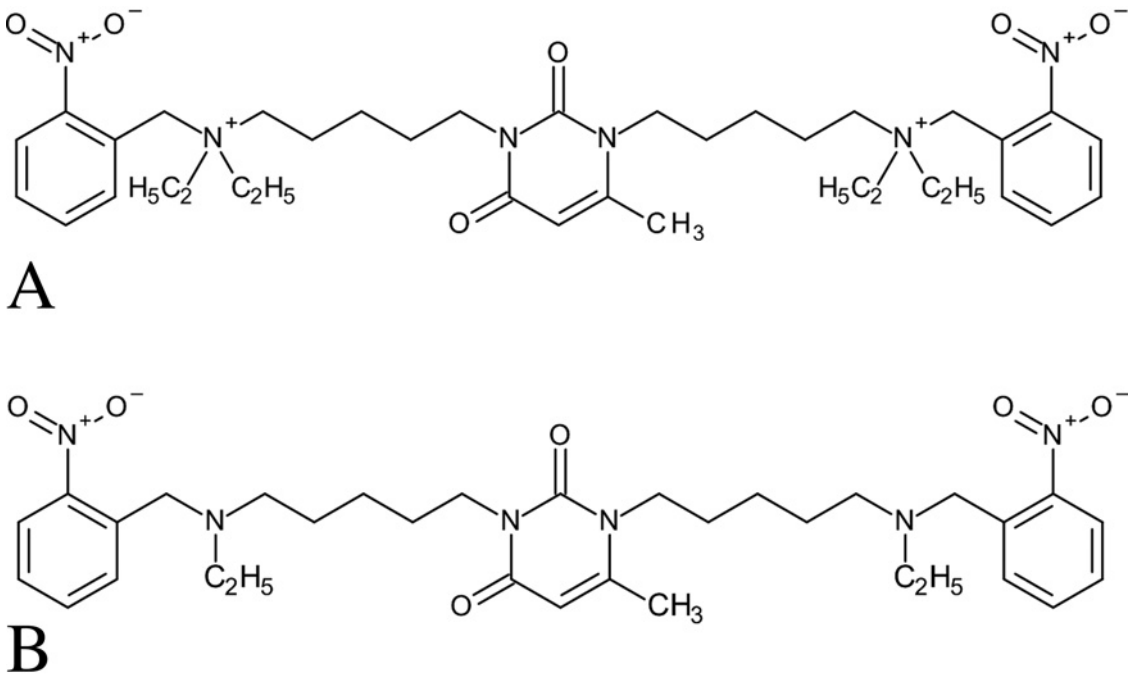

Figure 1 Structures of C-547 (A) and C-35 (B)

AChE is long (half-life of hAChE decarbamylation at 37 °C, $t_{\frac{1}{2}}$ = 26–28 min [9,10] at 25 °C, $t_{\frac{1}{2}}$ = 51 min [11]). Neostigmine (dimethyl carbamate, an analogue of pyridostigmine), also a non-specific ChE inhibitor, has the same half-life of decarbamylation and shorter pharmacokinetics than pyridostigmine [12]. However, because neostigmine causes strong muscarinic side effects, it is less widely used than pyridostigmine [13]. The third drug used is ambenonium. Although it is one of the strongest and highly selective reversible fast-binding inhibitors of AChE (K_i = 0.12 nM) [14], it is rarely used in clinical pharmacology for two reasons: (i) it has a short residence time on hAChE (τ = 2.7 min, $t_{\frac{1}{2}}$ = 1.9 min); and (ii) its pharmacokinetics are similar to those of pyridostigmine [12]. Because the number of specific AChE inhibitors for MG treatment is limited, research into new compounds is of great interest.

We previously described selective mammalian AChE inhibitors based on derivatives of the 1,3-bis[5-(*o*-nitrobenzylethylammonium)pentyl]-6-methyluracilic unit [15]. These inhibitors were tested in an animal model of MG and may be considered valuable candidates for the treatment of pathological muscle weakness syndromes [16]. In the present study, we investigated the mechanism of ChE inhibition by 1,3-bis[5(diethyl-*o*-nitrobenzylammonium)pentyl]-6-methyluracil dibromide (C-547), one of the most specific 6-methyluracil derivatives for AChE. The crystal structure of m (mouse) AChE and hAChE complexed with this inhibitor, and molecular modelling allowed us to depict the different steps of inhibition of hAChE. Comparison of inhibition and molecular modelling data for the non-charged related compound 1,3-bis[5(-*o*-nitrobenzylammonium)pentyl]-6-methyluracil dibromide (C-35) showed that the lack of quaternary nitrogen in the nitrobenzylammonium group abolishes slow-binding inhibition. This revealed the features that determine slow-binding inhibition (type B) of AChE: the bottleneck in the AChE gorge and quaternary nitrobenzylammonium group in the ligand. We showed that C-547 is a slow-binding reversible inhibitor of hAChE with one the highest known affinities. After formation of initial enzyme·inhibitor complex (K_i = 140 pM), an induced-fit step allows establishment of the final complex (K_i* = 22 pM). Estimated k_{off} is low, 0.05 min^{-1}. On the other hand, hBChE is reversibly inhibited by C-547 in a fast binding process with an affinity approximately four orders of magnitude lower than for hAChE. C-547, a highly selective slow-binding inhibitor of AChE, has a long target-residence time ($t_{\frac{1}{2}} \approx$14 min). Thus it is a promising drug for treatment of MG.

MATERIALS AND METHODS

Enzymes and chemicals

Recombinant hAChE was expressed in CHO (Chinese-hamster ovary) cells as described in [17]. hBChE was highly purified from human plasma as described in [18]. C-547 (681 Da, Figure 1A) was synthesized as described in [19] in the A.E. Arbuzov Institute of Organic and Physical Chemistry (Kazan, Russia). Its purity was >98 %. Stock solution (1 mM) of C-547 was prepared in water by weighing the dry powder. The structure of C-35 (non-protonated form, pK_{a1} = 6.49 and pK_{a2} = 5.28) is shown in Figure 1(B). Echothiophate was a gift from Biobasal. All other chemicals of biochemical grade were purchased from Sigma–Aldrich.

Active-site titration of enzymes

The number of active sites in the highly purified recombinant hAChE preparation was performed as described in [20]. Echothiophate was the titration agent. The AChE concentration [21] used in kinetic experiments was approximately 1 pM.

Kinetic analysis of ChE inhibition

ChE activities were assayed by the spectrophotometric method of Ellman et al. [21]. Measurements were performed on a PerkinElmer λ25 spectrophotometer at 412 nm and 25 °C in

50 mM sodium phosphate buffer (pH 8.0). The final volume in cuvette was 2 ml and the final concentrations: 0.25 mM DTNB, various concentrations of substrate (S), ACh or BCh (butylcholine) (0.01–1 mM) and inhibitor (I), C-547 (0.1–1 nM for inhibition of AChE and 0.1–10 μM for inhibition of BChE). Absorbance change was recorded for 10 min. The reaction was started with the addition of enzyme (AChE or BChE) into premixed substrate/buffer/inhibitor mixture. The final enzyme concentration in the assays was in the picomolar range. Thus inhibition experiments were always performed under pseudo-first-order conditions: [E]$<10\times$[I]. Controls of active enzyme (v_0) in the absence of inhibitor were performed for each set of experiments. Reaction mixture without enzyme served as a blank. For each condition, measurements were performed in triplicate or quadruplicate.

Determination of inhibition mechanism and inhibition constants

Measurements of initial reaction rates (v_0 and v_i, in the absence and presence of inhibitor, I, were used to determine fast reversible inhibition of AChE and BChE. Inhibition constants (means $\pm$ S.E.M.) for rapid reversible inhibition were determined from a Dixon plot ($1/v_i$ against [I]) and Cornish-Bowden transformation ([S]/v_i against [I]). Both plots also allowed the determination of the type of reversible inhibition [22]. Graphical analysis of plots was performed using Origin 8 software (Origin Lab).

With AChE (but not with BChE), there was a progressive decrease in activity in the presence of inhibitor before reaching a steady state. Therefore, to determine the mechanism of inhibition, the activity was recorded for 10 min until the steady state of inhibition (v_{ss}) was reached. Thus for AChE, values of v_i were used to fit integrated reaction rates as a function of time for different concentrations [S] and [I] (eqn 1):

$$[P]_t = v_{ss}t + \frac{(v_i - v_{ss})(1 - \exp^{-k_{obs}t})}{k_{obs}} \quad (1)$$

where $[P]_t$ is the concentration of released product of reaction, v_i is the initial velocity, v_{ss} is the steady state velocity after final equilibrium with inhibitor, and k_{obs} is the first-order rate constant corresponding to the slow-binding process of inhibitor. The progress curves for the slow phase of inhibition were analysed according to slow-binding inhibition methods [23–25]. Analysis of the dependence of the apparent first-order rate constant k_{obs} as a function of inhibitor concentration allowed us to determine the type of slow-binding inhibition and the binding kinetics parameters of C-547 to hAChE. Non-linear fitting of curves (k_{obs} against [I]) was carried out using Origin 8. Standard errors on mean values of elementary kinetic constants for the slow-binding step resulted from combined data of repeat experiments. Errors on complex kinetic and binding constants were determined taking into account propagation of errors [26].

Crystal structure of mAChE in complex with C-547

Crystals of mAChE were grown as described previously [27]. Crystals of *apo*-mAChE were soaked for 10 min in a mother liquor solution (0.1 M Tris/HCl, pH 7.4, and 1.6 M ammonium sulfate) containing 1 mM C-547 for forming the complex. After soaking, crystals were washed in a cryoprotective solution (0.1 M Tris/HCl, pH 7.4, 1.8 M ammonium sulfate and 18 % glycerol) and then flash-cooled in liquid nitrogen.

Diffraction data were collected on the ID14-1 beamline at the European Synchrotron Radiation Facility (ESRF, Grenoble, France) with an ADSC Quantum Q210 detector. The beam was characterized by a wavelength of 0.9334 Å and the crystals were held at 100 K during data collection. The diffraction data were processed with XDS [28], intensities of integrated reflections were scaled using XSCALE, and structure factors were calculated using XDSCONV. The structures were solved by molecular replacement with the program MOLREP [29], using PDB entry 4A16 as the starting model. C-547 and its topological descriptions were built using Phenix elbow. The initial model was refined by iterative cycles of model building with Coot [30], and a refinement strategy involving TLS (Translation–Libration–Screw-rotation), Ramachandran, secondary-structure restraints and occupancy optimization with Phenix [31]. Successive alternation of refinement cycles and manual model building were performed until R_{work} and R_{free} did not decrease any further. A feature-enhanced map was calculated at the latest stage using phenix.fem to help resolve remaining poorly defined regions of the model [32]. Protein structures were illustrated using the program PyMOL (http://www.pymol.org).

Molecular modelling

Protein model preparation

X-ray structures of hAChE reported in [33] were used (PDB codes 4EY4–4EY8). These structures lack loop fragments 259–264 and 495–497. These were inserted from another hAChE X-ray structure (PDB code 4BDT [34]). Hydrogen atoms were added with respect to the hydrogen-bonding network by Reduce software [35]. All five structures were used as targets for molecular docking.

For MD simulation hAChE, X-ray structures 4EY4 and 4EY7 were pre-optimized. Water and ions were added (see details on MD systems set-up and simulation details below), and coordinates of all atoms found in X-ray structure were fixed. Positions of all added atoms were minimized in 5000 steps and subjected to 5 ns MD simulation to optimize water box and added loops. Then, all atoms were minimized in 5000 steps. Preparation and optimization of BChE structure is described in [36].

Molecular docking

Molecular docking with an LGA (Lamarckian Genetic Algorithm) [37], was performed with Autodock 4.2.6 [38] software. Grid box for docking of 30 Å$\times$30 Å$\times$30 Å included the whole gorge from the mouth to the active site, including the PAS (peripheral anionic site). The main of selected LGA parameters were as follows: 256 runs, 25×10^6 evaluations, 27×10^4 generations and population size 300. For the best docked positions, 256 additional runs of LS (local search) were performed. For comparison of binding affinity between different snapshots of MD simulations, the protein–ligand complex from the snapshot was minimized molecular-mechanically and binding energy was estimated by LS run. Open Babel [39] software was used for format conversion.

MD simulation

For all MD simulations, NAMD 2.10 software [40] with a CHARMM36 force field [41] was used. MD simulations were run at the Lomonosov Moscow State University supercomputer [42]. For the preparation of the model systems and further analysis of MD trajectories, VMD software [43] was used. For all protein

systems and protein–ligand systems, a TIP3P water box was added with boundaries at least 10 Å from protein and ligand atoms. Na^+ and Cl^- ions were added to the final ion concentration of 0.15 M. MD runs were performed in NPT ensemble with 298 K, 1 atm (101.325 kPa), periodical boundary conditions.

Ligand parameterization

For molecules C-547 and non-protonated form of C-35, parameters were taken from the Charmm General Force Field [44]; certain parameters, which were not available there, were parameterized according to the procedure described in [45,46] with quantum calculations at MP2/6-31G* and HF/6-31G* for atomic partial charge optimization.

Unconstrained MD

Structures of (i) docked complex of hAChE and C-547; and (ii) hAChE with C-547 placed at the entrance to the gorge at a distance of 22 Å from the bottom, were surrounded by a saline solution box, which was equilibrated with protein and ligand atoms fixed for 5 ns. System (i) 67444 atoms 79 Å×82.5 Å×98.5 Å, and (ii) 108265 atoms 107 Å×92.5 Å×107 Å simulation box sizes after equilibration. Then, all atoms of the systems were minimized in 5000 steps. Unconstrained MD simulation was run for 50 ns for the docked hAChE–C-547 complex and 500 ns for C-547 placed at the entrance to the gorge. For simulation of C-547 roaming on the enzyme surface towards the PAS, access into the gorge was limited with the *colvars* module.

Steered molecular dynamics (SMD)

SMD force application vector was determined between Glu^{202} C^{δ} atom and the centre of the bottleneck determined using Caver Analyst software [47]. The ligand was placed with the TAA (tetraalkylammonium) group nitrogen atom on this vector at 23 Å distance, pulling force was applied to this atom with constant velocity 1 Å/ns, force constant was adjusted in series of test runs and set to 5 kcal/mol·Å^2 (1 kcal = 4.184 kJ), and Glu^{202} C^{δ} atom was fixed. To avoid displacement of the protein due to pulling force, 5 kcal/mol·Å^2 harmonic restraints were applied to C^{α} atoms of peripheral amino acids Leu^{22}, Val^{147}, Val^{226}, Leu^{269}, Leu^{380}, Leu^{414} and Gln^{474}. For pulling C-547 out from the protein–ligand complex, force was applied in the reverse direction to the nitrogen atom of the further from the active-site TAA group. For SMD with BChE, forces and restraints were applied to the corresponding residues from alignment of hAChE and hBChE sequences.

RESULTS

Fast reversible inhibition of hAChE

Kinetic analysis of inhibition of hAChE by C-547, i.e. v_i as a function of [I], showed that the enzyme is first rapidly inhibited. The reversible inhibition is of mixed type with a strong affinity: $K_i = 140 \pm 16$ pM and $K_i' = 530 \pm 40$ pM, corresponding respectively to dissociation of the enzyme·inhibitor (EI) complex and dissociation of the enzyme·substrate·inhibitor complex (ESI) (Supplementary Figure S1). In a previous paper, we reported that C-35 is a classical mixed-type fast inhibitor of hAChE with K_i = 2.7 nM and $K_i' = 5.7$ nM [47].

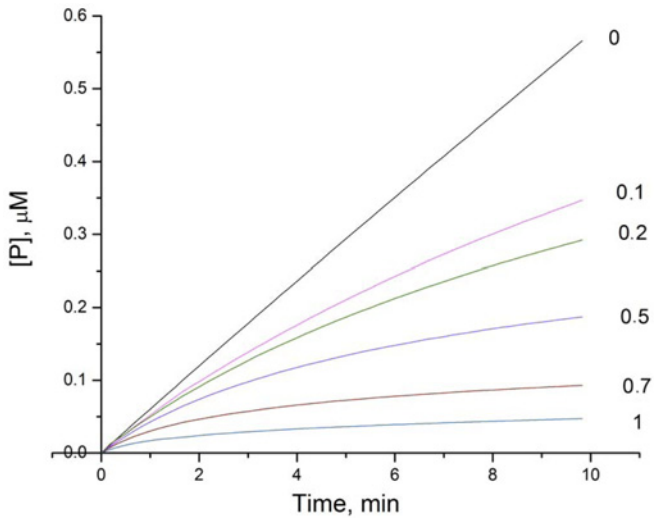

Figure 2 Progress curves for slow-binding inhibition of hAChE by C-547 at pH 8.0 and 25 °C

C-547 concentrations ranged from 0.1 to 1 nM.

Slow-binding inhibition of hAChE

The fast inhibition phase (formation of EI and ESI) with C-547 was followed by a slow-binding inhibition phase (formation of EI*) until a new equilibrium, i.e. steady state, was reached (Figure 2). Eqn (1) describes this slow process. The dependence of the pseudo-first-order constant (k_{obs}) on inhibitor concentration was determined (Figure 2). Hyperbolic upward curved plots in Figure 2 clearly demonstrate that slow-binding inhibition of hAChE obeys the mechanism of slow-binding inhibition of type B, i.e. rapid formation of the initial enzyme·inhibitor complex EI that slowly isomerizes into EI* according to the model:

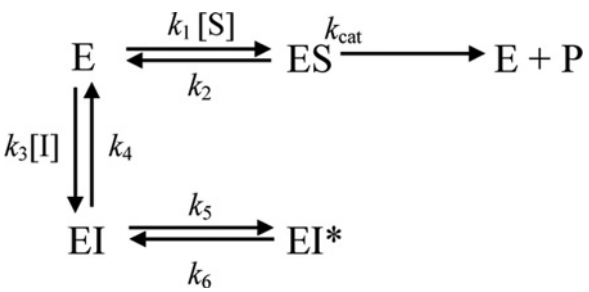

At low substrate concentration when there is no inhibition of AChE by excess substrate of, i.e. at ACh ⩽1 mM, the initial velocity in the presence of inhibitor (v_i) is:

$$v_i = \frac{V_{max}[S]}{K_M(1 + [I]/K_i) + [S]} \quad (2)$$

The steady-state velocity (v_s) in the presence of inhibitor is:

$$v_s = \frac{V_{max}[S]}{K_M(1 + [I]/K_i^*) + [S]} \quad (3)$$

and the pseudo-first-order constant (k_{obs}) for the slow-binding step is:

$$k_{obs} = k_6 + \frac{k_5[I]}{K_i\left(1 + \frac{[S]}{K_M}\right) + [I]} \quad (4)$$

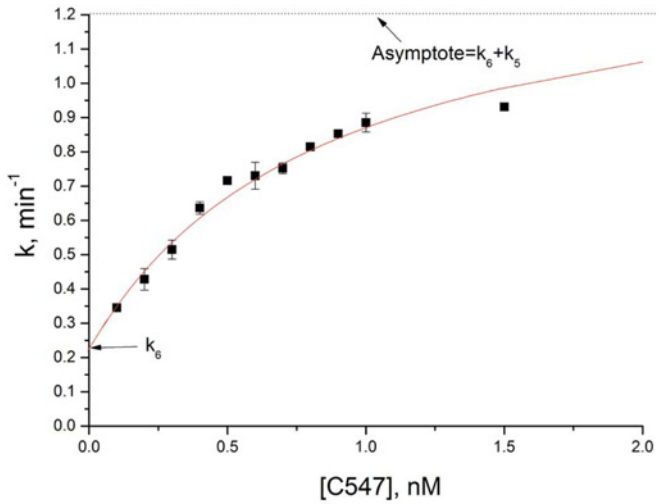

Figure 3 C-547 concentration-dependence of the apparent first-order inhibition constant, k_{obs}, for slow-binding inhibition of hAChE

with

$$K_i = k_4/k_5 \quad (5)$$

and

$$K_i^* = K_i\,[k_6/(k_5 + k_6)] \quad (6)$$

Slow-binding inhibition parameters were calculated from the plot in Figure 3, according to eqns (4), (5) and (6). They are: $k_5 = 1.192 \pm 0.037$ min^{-1}, $k_6 = 0.222 \pm 0.014$ min^{-1}, and $K_i^* = 22 \pm 1.13$ pM. Thus isomerization of the enzyme·inhibitor complex led to an increase in binding affinity of approximately one order of magnitude. In addition, for mechanism B, the overall rate of dissociation of the enzyme·inhibitor complex, k_{off}, is:

$$k_{off} = \frac{k_4 k_6}{k_4 + k_5 + k_6} \quad (7)$$

The reciprocal, $\tau = 1/k_{off}$, is the residence time of the enzyme·inhibitor complex. Because molecular modelling showed that C-547 sticks on the surface of the enzyme beyond the rim of the gorge on multiple non-specific binding sites as a polyelectrolyte does (see the 'Dynamics of C-547 roaming outside the gorge' section below), it has to slide slowly to bind to the PAS, the initial specific binding site. Therefore, although the PAS is solvent-exposed, we may assume that the association rate constant of this bulky alkylammonium derivative of 6-methyluracil is much lower than the diffusion-controlled limit for a second-order rate constant for enzyme reactions, i.e. 10^9 M^{-1}·s^{-1}. Most k_{on} values for binding of small drugs to macromolecular targets range between 10^6 and 10^8 M^{-1}·s^{-1} [24]. For instance, k_{on} of the bis-alkylammonium ambenonium (537.5 Da), to hAChE is 5.2×10^7 M^{-1}·s^{-1} [14]. Thus, taking into account the chemical structure and K_i of both alkylammonium compounds, ambenonium compared with C-547 (120 pM compared with 140 pM), it may be reasonably assumed that the second-order association rate constant of C-547 to the PAS of hAChE is close to the k_{on} value of ambenonium. Taking $k_{on} \approx 5\times10^7$ M^{-1}·s^{-1}, it follows that $k_4 \approx 0.42 \pm 0.04$ min^{-1}. This leads to $k_{off} \approx 0.051 \pm 0.027$ min^{-1} and $\tau \approx 20 \pm 11$ min and the half-life for dissociation of the inhibitor $t_{\frac{1}{2}} = \ln 2/k_{off} \approx 14 \pm 8$ min.

At this point, we must stress that both the residence time and pharmacokinetics parameters, i.e. the drug concentration in target compartment against time, determine the duration of efficacy of a drug in the body. Thus the pharmacological efficacy depends on the fractional occupancy of the enzyme as a function of time. For slow-binding inhibition that follows mechanism B, the fractional occupancy at any time, FO_t, depends on $[I]_t$ and on the inhibition kinetics constants k_3, k_4, k_5 and k_6 as follows [24,48]:

$$FO_t = \frac{[I]_t}{[I]_t + \dfrac{k_4}{k_3 + \frac{k_3 k_5}{k_6}}} \quad (8)$$

Thus, for a concentration of C-547 close to K_i^* at the neuromuscular junction, i.e. 10^{-11} M, the mean value of $FO_t \approx 30\,\%$. For concentrations 10- and 100-fold higher (enzyme saturation), the mean values of FO_t are 82 and 98 % respectively.

Fast reversible binding of hBChE

Unlike hAChE, inhibition of hBChE did not show any time-dependence. The enzyme was reversibly inhibited by C-547 in a fast equilibrium. Inhibition of the enzyme is mixed-type competitive with inhibition constant $K_i = 1.77 \pm 0.11$ μM and $K_i' = 3.17 \pm 0.20$ μM (Supplementary Figure S2). Thus the affinity of C-547 (reversible fast inhibition) for hBChE is approximately four orders of magnitude lower than for hAChE.

C-35 was found to be a mixed-type inhibitor of hBChE with $K_i = 13.6$ μM and $K_i' = 22.3$ μM [47]. Thus not only does C-35 not behave as a slow-binding inhibitor of AChE, but also C-35 is less selective than C-547 for AChE (selectivity ratio BChE/AChE $\approx$ 5000).

X-ray structure of the mAChE–C-547 complex

To investigate the interactions involved in the formation of the reversible complex, we solved the crystal structure of mAChE with C-547 (PDB code 5FKJ). mAChE was chosen, as it is a mammalian enzyme structurally close to hAChE (88 % sequence homology) and it generally crystallizes more easily than hAChE in our hands. The structure of the mAChE–C-547 complex was solved at 3.13 Å resolution. Data and refinement statistics are detailed in Table 1.

Electron density spanning the entire active site gorge and corresponding to C-547 could be identified in all four monomers present in the asymmetric unit. The ligand could be fully modelled for monomers A and C, but due to high disorder, no density could be clearly attributed to the *o*-nitrobenzylammonium group located at the gorge entrance for monomers B and D. Indeed, this part of the ligand is solely stabilized in monomer A (or C) where loop 257–265 of monomer D (or B) is docked at the peripheral site as shown in Figure 4. This suggests that the peripheral *o*-nitrobenzylammonium group is not mandatory to achieve nanomolar affinity. By contrast, the *o*-nitrobenzylammonium group located deep in the gorge is well stabilized by T-stacking aromatic interaction with Trp^{86}, hydrogen-bonding of the nitro group to the hydroxy group of Tyr^{124} (3.1 Å), and cation–π interactions with Tyr^{337} and Tyr^{341}. Above the gorge bottleneck shaped by Tyr^{124} and Tyr^{341}, the 6-methyluracil subpart is stabilized by aromatic stacking interactions with Trp^{286} of the PAS, and a hydrogen bond between a carbonyl and the main-chain nitrogen of Phe^{295} (2.8 Å). This hydrogen bond allows the resolution of the orientation of the ligand into the gorge because the methyl group of uracil would be unfavourably facing the

Table 1 Data collection and refinement statistics

PDB entry code	5fkj
Wavelength	0.9334
Resolution range (Å)	87.72 - 3.13 (3.24 - 3.13)
Space group	$P2_12_12_1$
Unit cell parameters (Å)	137.15, 175.45, 224.4
Total reflections	355989 (34232)
Unique reflections	95147 (9123)
Multiplicity	3.7 (3.7)
completeness (%)	99 (97)
I/s(I)	10.7 (1.6)
Wilson B-factor	65.98
R_{merge} (%)	0.137 (0.842)
R_{meas} (%)	0.160 (0.983)
$CC_{1/2}$	0.99 (0.664)
CC*	0.998 (0.893)
Reflections used in refinement	94994 (9122)
Reflections used in refinement R_{free}	1046 (101)
Redundancy	0.006
R_{work} (%)	0.207 (0.343)
R_{free} (%)	0.249 (0.375)
CC(work)	0.947 (0.759)
CC(free)	0.916 (0.717)
Number of non-hydrogen atoms	17437
macromolecules	16776
ligands	287
protein residues	2155
RMS bonds (Å)	0.004
RMS angles (deg)	0.85
Ramachandran favoured (%)	97
Ramachandran allowed (%)	2.8
Ramachandran outliers (%)	0.23
Rotamer outliers (%)	1.9
Clashscore	6.0
Average B-factor (Å^2)	71.5
macromolecules	71.8
ligands	79.4
solvent	51.7
Number of TLS group	4

Statistics for the highest-resolution shell are shown in parentheses.

main-chain nitrogen if the orientation of C-547 were inversed in the model.

Molecular modelling of C-547 and C-35 binding to hAChE and hBChE

Molecular docking results of C-547 to several available X-ray structures of hAChE and hBChE are described in the Supplementary Online Data and presented in corresponding Supplementary Figures S3 and S4. Molecular docking of C-547 to the mAChE X-ray structure was reported previously [16].

Complex of C-547 with the hAChE PAS

With the ligand placed at the entrance of the AChE gorge for 0.5 μs of unconstrained MD simulation, the ligand reaches the PAS rather quickly, within 50 ns of simulation (Supplementary Figure S5). The *o*-nitrobenzylammonium group interacts mainly with Trp^{286}, Tyr^{341} and Tyr^{124}. Tyr^{341} and Tyr^{124} are oriented across the gorge, forming the bottleneck gate. After formation of complex with the PAS, the ligand does not move significantly.

Binding affinity was estimated for snapshots over the trajectory with the lowest energy of -11.90 kcal/mol for snapshot at 430 ns; the complex is shown in Supplementary Figure S5(B). For comparison, molecular docking of C-547 into the PAS of hAChE X-ray structures gave the best binding affinity, -9.51 kcal/mol for *apo*-hAChE (PDB code 4EY4).

Trafficking of C-547 along the hAChE gorge

The 500 ns unconstrained MD simulation showed rapid formation of complex between C-547 and the PAS and subsequent fine adjustment of the initial complex; however, passing through the bottleneck would require a much longer simulation time. The conventional approach to explore this process is to force the inhibitor along the gorge at constant velocity by applying an external pulling force [40,49]. The reverse process of protein–ligand complex dissociation was modelled by sucking C-547 out from hAChE. Rupturing force was applied, starting from the snapshot presented in Supplementary Figure S3(B). The reaction co-ordinate, or position of the ligand inside the AChE gorge, is defined as the distance between the Glu^{202} carboxy group, located at the bottom of the gorge and the ligand TAA head. In order to relate the SMD pulling in and extraction force profiles obtained (Figure 5) to the actual position in the gorge, distance is shown on the *y*-axis, force is on the *x*-axis.

For SMD pulling in, pathway barrier **1** of 350 pN at level of 15 Å corresponds to transit of the C-547 headgroup through the PAS during unconstrained MD presented in Figure 6. The barrier occurs due rupture of π–cation interaction between positively charged TAA group and Trp^{286} (Figure 6A) under the non-equilibrium influence of pulling force. Next higher barrier **2** of 500 pN corresponds to penetration of the headgroup through the bottleneck (Figure 6B), namely passing of the *o*-nitrobenzylammonium group across the Tyr^{124}/Tyr^{341} gate. Tyr^{124} is contorted and displaced downwards, driven by the ligand. Once the bottleneck is passed, the system falls into a very deep potential well **3** at a level of 9–10 Å from the gorge bottom with TAA group below Tyr^{341} and Tyr^{124}, at the level of Tyr^{337}. This position inside hAChE is very similar to the above-described X-ray structure of the mAChE–C-547 complex. Previous SMD simulation with mAChE [25] gave similar results.

To relieve strain, induced by pulling force, unconstrained MD from position **3** was performed for 10 ns with LS binding affinity estimation for the snapshot ensemble. The lowest binding energy was -14.48 kcal/mol, corresponding to $K_i = 24.3$ pM for the snapshot at 5.6 ns of unconstrained MD (-14.27 kcal/mol for modelling with mAChE). LS for X-ray position provided estimation of binding energy of -10.68 kcal/mol for monomer A, and -11.05 kcal/mol for monomer C in the asymmetric unit (see the 'X-ray structure of the mAChE–C-547 complex' section). Indeed, the crystallized protein has a rigid structure, and no changes in backbone conformation compared with the *apo* state can be observed. Binding of C-547 to the mAChE crystal results only in rotation of the side chains of Trp^{286}, Tyr^{341} and Tyr^{337}. MD simulation of the flexible protein in water at room temperature allows better accommodation of the ligand in the gorge.

The position of C-547 from X-ray structure with mAChE (Figure 7A), and from MD simulation with hAChE (Figure 7B) and mAChE (Figure 7C), shows the same interactions below the bottleneck, hitherto described in section X-ray structure of mAChE-C-547 complex. Part of the ligand located above the bottleneck has higher mobility, also observed by crystallography.

The active site located at the bottom of the gorge is isolated by a much higher barrier **4** corresponding to passing by Tyr^{337} and Phe^{338} and squeezing the *o*-nitrobenzylammonium group into the tight compartment of the active site and its adjacent anionic

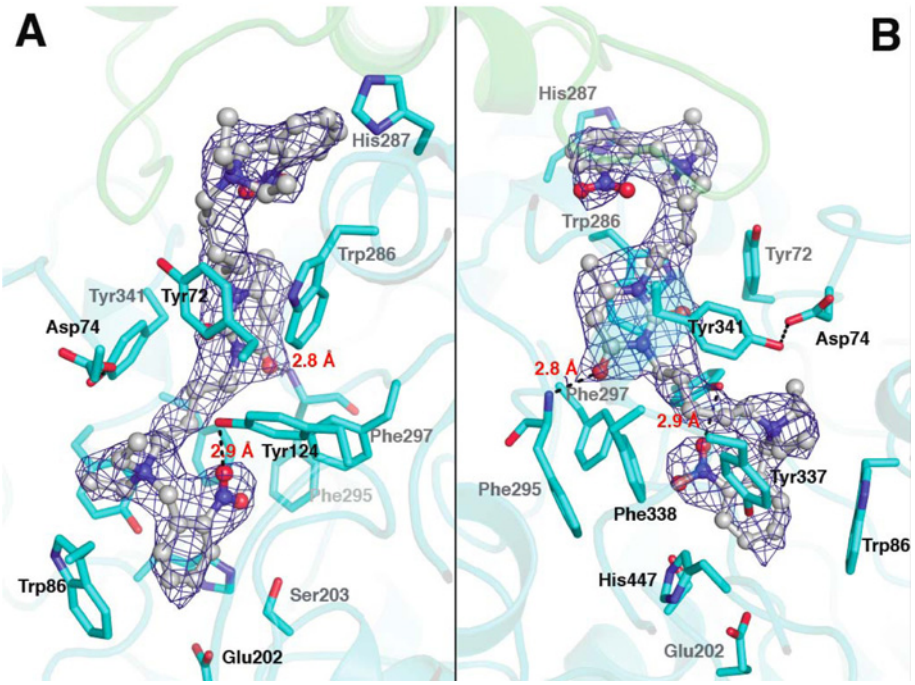

Figure 4 Complementary views (A and B) of C-547 bound in the active-site gorge of mAChE (PDB code 5FKJ, chain A)

The main interactions consist in aromatic stacking with Trp^{86} and Trp^{286}, cation–π interactions with Tyr^{337} and Tyr^{341}, and hydrogen-bonding to Tyr^{124} and Phe^{295} (broken lines; distances in red). A loop from chain D (green cartoon representation) stabilizes the external part of C-547. A feature enhanced map calculated using phenix.fem is represented as a blue mesh around the ligand (2σ level).

subsite. A long time is needed to reach the active site, a duration far longer than the incubation time (10 min) required for diffusion in crystal for the X-ray structure.

SMD modelling of the association and dissociation processes allows comparison of both processes. To disrupt interactions established in the equilibrated protein–ligand complex and to overcome the bottleneck gates in the opposite directions, much higher rupturing forces are needed. This balance of maxima of pulling in and rupturing forces corresponds to the values obtained in an earlier SMD study for huperzine A, a slow-binding inhibitor of AChE, with applied forces of 360 pN and 820 pN for association and dissociation with/from *Torpedo californica* AChE respectively [49].

Dynamics of C-547 roaming outside the gorge towards the PAS

Figure 5 shows that the PAS may be practically limited at a distance of 22 Å from the gorge bottom. Special MD simulation of C-547 roaming outside the gorge with restriction on entering the PAS was performed. Figure 8 shows that that C-547 stays very close to the surface of the protein beyond the rim of the gorge. It can be seen in Figure 8(A) that when distance is less than 32 Å from the active site, protein and ligand are always in contact through non-specific ionic interactions, with the ligand acting like a polyelectrolyte. Such a distance is greater than the PAS topological limit. Then, the ligand can be effectively considered in bulk solvent when the distance is greater than 45 Å. C-547 can stick to various non-specific sites on the protein surface, with two of them shown in Figure 8(B): the position shown in magenta has the maximum number of contacts, and the position shown in pink belongs to the high-density area of Figure 8(A) at 33 Å distance. Approaching the entrance of the gorge, right above the PAS, due to strong electrostatic field, C-547 is erected. This results in lesser contacts with the protein (position coloured cyan). This indicates that entering the PAS has a certain potential barrier. In conclusion, multiple non-specific contacts with the enzyme surface in the approach to the PAS affect k_{on} as stated in the section slow-binding inhibition of hAChE.

Trafficking of C-547 along the hBChE gorge

Calculated SMD pulling in and extracting force profiles for C-547 with hBChE compared with hAChE are presented in Supplementary Figure S6. Force profiles for BChE are much lower and do not have a peaks corresponding to crossing the bottleneck. The pulling in process has a distinct, but still rather low, force peak, which can be attributed to disruption of contact with Tyr^{332}, as for force peak **1** (i.e. disruption of π–cationic contacts with the hAChE PAS aromatic residues in Figures 5 and 6A). Owing to narrowing of the gorge, the pulling force is increasing when ligand is approaching the bottom. In this area, both gorges of hAChE and hBChE have a similar shape and size (Supplementary Figure S7). However, owing to strong binding below the bottleneck (position **3** in Figures 5 and 7), the pulling force required for hAChE is much higher than for hBChE. Accordingly, owing to much weaker binding of C-547 to hBChE, breaking forces needed to extract it from the gorge are much lower than those for extracting C-547 from hAChE (Supplementary Figure S6B).

Trafficking of C-35 down the hAChE gorge

The pK_a of C-35 determined by pH-metric titration gave two values, 5.28 and 6.49 [50]. In the present study, only MD results for non-protonated form of C-35 are reported. Calculated SMD pulling in and extracting force profiles for C-35 compared with

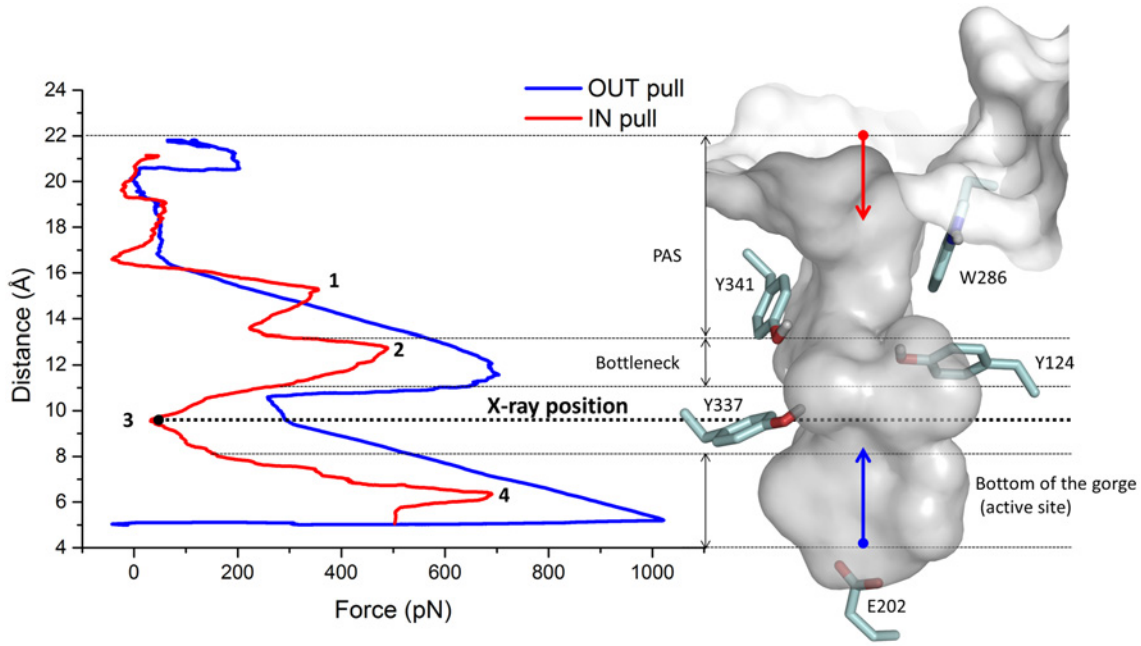

Figure 5 Force profile for pulling of compound C-547 corresponding to the hAChE gorge

Red line for pulling in (red arrow shows direction), blue line for extracting from the active site (blue arrow shows direction). Force is averaged over 1 ns of the SMD simulation.

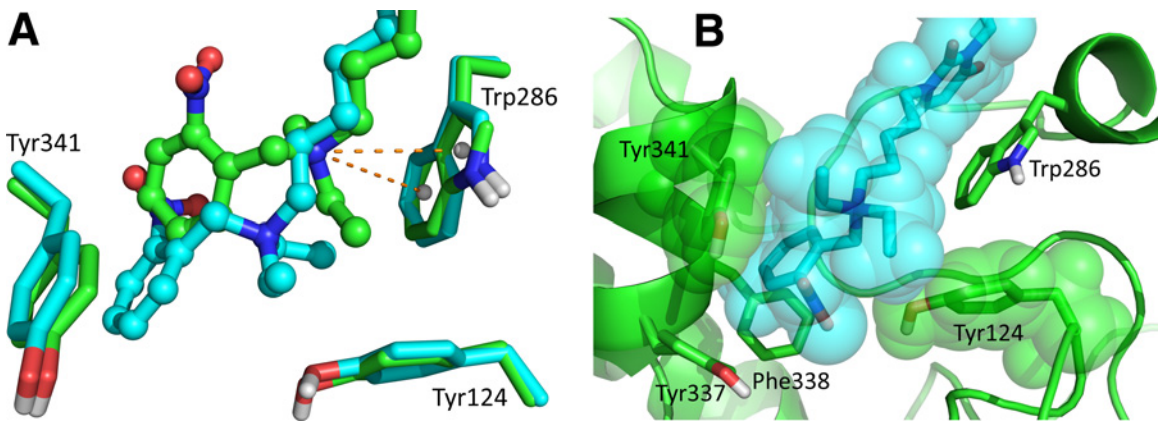

Figure 6 Compound C-547 overcoming hAChE bottleneck

(**A**) Displacement corresponding to SMD barrier **1**, from green to cyan. (**B**) C-547 headgroup passing the bottleneck; the snapshot corresponds to the moment of maximum applied pulling force **2**.

C-547 with hAChE are presented in Supplementary Figure S8. Owing to the absence of a quaternary ammonium group, there is no force intensity peak corresponding to peak **1** for C-547 (see above). However, the force peak for crossing the bottleneck is close to force peak **2**. Most importantly, for C-35 that crossed the bottleneck, there is no deep potential well **3**. Indeed, in the absence of positive charge, the tertiary nitrobenzylammonium group does not bind tightly to the area below the bottleneck. This means that there is no driving force for C-35 to cross the bottleneck. Force profiles for extracting of C-35 from hAChE and hBChE also support the importance of the quaternary nitrogen positive charge for binding.

DISCUSSION

hAChE is reversibly inhibited by C-547 in a slow-binding process of type B. Slow-binding inhibition of type B results from isomerization of enzyme·inhibitor complex [23,24]. In fact, molecular modelling showed that 'isomerization' corresponds to induced-fit transfer of the inhibitor from the initial binding position in the upper part of the gorge to the final binding position at the bottom of the gorge. Owing to the presence of the bottleneck in the middle of the gorge, acting under conformation gating, fast transfer of bulky inhibitor is impaired. Thus an induced-fit step is needed for final accommodation of C-547. The initial enzyme complex (K_i = 140 pM) induced-fit step allows establishment of the final complex (K_i^* = 22 pM). The estimated k_{off} is low, at 0.051 min^{-1}.

hBChE is reversibly inhibited by C-547 with an affinity of approximately four orders of magnitude lower than the affinity of hAChE. The lowest affinity of BChE for C-547 is due to the presence of only one aromatic residue (Tyr^{332}) in the PAS of BChE compared with that of AChE, and the absence of most aromatic residues along the active site gorge. In addition, the

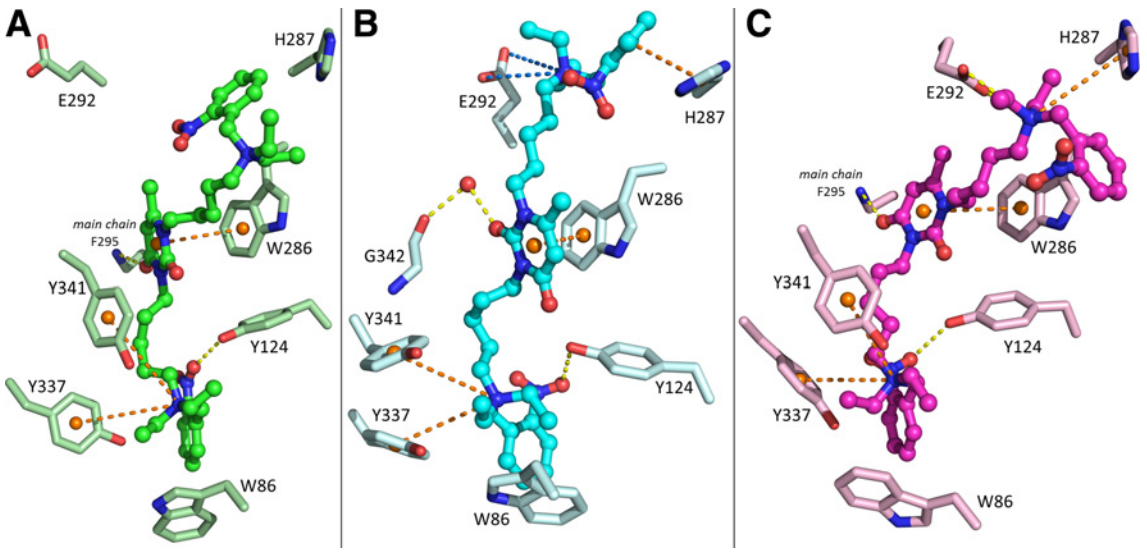

Figure 7 Comparison of crystallographic and molecular modeling complexes of compound C-547 with AChE

(**A**) Complex of C-547 with crystallized mAChE. Position of C-547 after crossing of the bottleneck of hAChE (**B**) and mAChE (**C**), corresponding to the minimum of pulling force after equilibration. Main interactions are shown with broken lines, yellow for hydrogen bonds, orange for π interactions, blue for the ion pair. Interactions of C-547 part located below the bottleneck are identical in X-ray and both MD snapshots. Owing to increased mobility and induced fit, there are some differences between crystal structure and MD snapshots above the bottleneck. In snapshots for hAChE and mAChE with the highest estimated affinities, the TAA group located at the entrance of the gorge forms an ion pair with Glu^{292}, and the *o*-nitrobenzyl ring forms π-stacking interactions with the His^{287} imidazole ring in hAChE and π–cation interactions in mAChE. Some difference originates from two possible orientations of the 6-methyluracil ring: in hAChE, it forms a hydrogen bond through a water molecule with Gly^{342} oxygen atom, and in mAChE, it forms a hydrogen bond with the main-chain nitrogen of Phe^{295}. This difference does not affect the binding affinity. Separate MD runs show that the orientation of the 6-methyluracil ring is of a random nature.

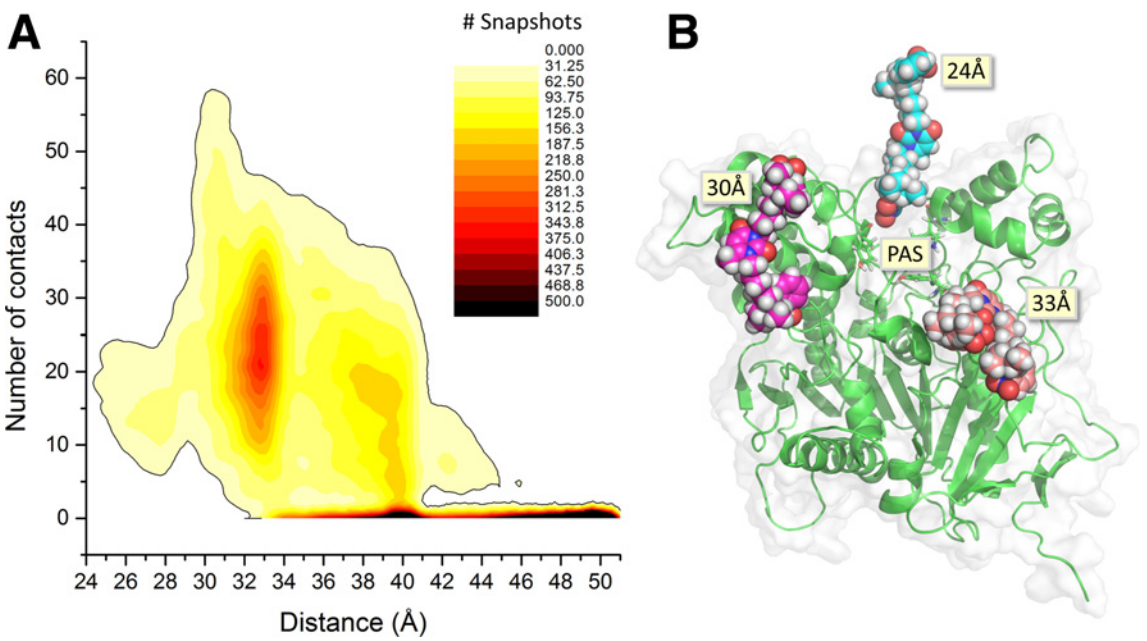

Figure 8 Non-specific contacts between C-547 and the hAChE surface

(**A**) Distribution of the number of contacts between C-547 and the hAChE surface as a function of distance from the bottom of the gorge during 80 ns MD simulation (the simulation was performed with restriction for the ligand entering the PAS, i.e. approach at a distance of less than 24 Å). The distance between the ligand and the active site was measured as above as the distance between the nitrogen atom of one TAA group and the Glu^{202} carboxy group. Contact is defined as a pair of atoms belonging to protein and ligand respectively within 3 Å of each other. Statistics were gathered for 80000 snapshots, and the density threshold was set at the level of 500 snapshots for plot readability. (**B**) A few locations of ligand roaming on the hAChE surface are shown as examples.

active-site gorge of BChE is larger than that of AChE (500 Å^3 compared with 300 Å^3) [51] with no bottleneck at half-way. In particular, the gate residue Tyr^{124} in hAChE is Gln^{119} in hBChE. Then, BChE does not display a slow-binding process. A way to validate modelling about the bottleneck crossing could have been to study the binding of C-547 after site-directed mutagenesis of key residues, including Tyr^{124}, in hAChE. However, attempts to convert hAChE into hBChE by mutagenesis of active-site gorge

residues, i.e. 'butyrylization', did not lead to mutants displaying binding (k_{on}) and dissociation (k_{off}) rate constants similar to those of BChE with the transition state analogue TMTFA [*m*-(*N*,*N*,*N*-trimethylammonio)trifluoroacetophenone], a slow-binding inhibitor. It was concluded that mutagenesis failed to create the functional architecture of the BChE active-site gorge needed for fine adjustment of the inhibitor to mimic the transition state of substrate [52]. This failure emphasizes the limitation of the mutagenesis approach for studies of slow-binding inhibitions, involving fine MD for induced-fit adjustments. However, we may consider hBChE itself as a maximal mutant of hAChE, and compare kinetics and SMD results for both of them. Indeed, hAChE and hBChE share 53 % sequence homology [53]. In general, sequence differences determine alterations in overall protein dynamics. More specifically, replacement of six aromatic residues with smaller ones results in a larger size and modified shape of the BChE gorge (Supplementary Figure S7), whereas the lowest part of their gorge remains similar. Comparison of calculated force profiles for pulling C-547 down and extracting it from the gorge of hAChE and BChE (Supplementary Figure S6) emphasizes the role of specific amino acids in the gorge and explains why BChE does not display slow-binding inhibition kinetics with C-547.

An inhibition study with the variant compound C-35 reveals another side of the process: the role of the cationic TAA group in slow binding. Compound C-35 and its uncharged form were described in [50] with particular attention to their interactions with the PAS. Possible binding positions in the active site were also obtained, but accessibility to these positions was disputed. The calculated force profile for C-35 shows that crossing over the bottleneck is unlikely. Instead, C-35 forms a complex with the PAS in a fast process.

Summing up information obtained from inhibition kinetics of C-547 and its uncharged analogue C-35 with hAChE and its sister enzyme hBChE, the X-ray structure of C-547 with mAChE, and corresponding SMD modelling, we can list the following factors that determine the slow-binding inhibition: (i) rapid formation of complex EI between aromatic residues of AChE in the PAS and cationic TAA group; (ii) slow crossing of the AChE bottleneck induced by attraction of the TAA group by the underlying residues; (iii) EI* results from tight binding between cationic TAA group and *o*-nitrobenzyl ring, and aromatic residues of the gorge. In the absence of positive charge on the nitrobenzylammonium group, or absence of bottleneck as in BChE, inhibition loses its slow-binding nature. With fewer aromatic residues in the gorge, binding becomes far less tight.

The high selectivity for AChE is the main advantage of C-547 for MG treatment. Low k_{off}, i.e. long residence time ($\tau = 1/k_{off}$) or long half-life ($t_{\frac{1}{2}} = \ln 2/k_{off}$) on AChE is another advantage of C-547. Indeed, k_{off} and τ reflect the occupancy time of the inhibitor on the target [24]. Both the residence time and pharmacokinetics parameters, in particular the drug concentration in the target compartment against time, determine the duration of efficacy of a drug in the body. There is an interplay between inhibition kinetics, pharmacokinetics and pharmacodynamics, so that the pharmacological efficacy depends on the fractional occupancy of the enzyme as a function of time. For long residence times, the fractional occupancy time can remain high for a long time even though the effective concentration of inhibitor is rapidly decreasing because of fast pharmacokinetics. Thus these parameters provide a measure of the duration of toxic and pharmacodynamic effects. A drug with rapid pharmacokinetics but with a long residence time on target will have prolonged effects, a better efficacy with lesser side effects, i.e. a better safety compared with high off-rate inhibitors. Thus selective low off-rate inhibitors present pharmacological advantages over fast reversible inhibitors. This statement must be balanced by pharmacokinetics. In the case of the fast-binding reversible inhibitor of AChE, ambenonium, that displays a short residence time on AChE ($\tau = 2.7$ min) and relatively fast pharmacokinetics (mean residence time in the rat bloodstream of 20–30 min) [54], C-547 may present advantages for improved treatment of MG: (i) long residence time on target; and (ii) slower pharmacokinetics with prolonged pharmacological effects.

Conclusion

C-547 presents significant advantages over drugs that are currently used for MG treatment. Highly selective slow-binding inhibition of hAChE with a long target residence time ($\tau = 20$ min) or $t_{\frac{1}{2}} = 14$ min at 25 °C compared with $t_{\frac{1}{2}} = 2$ min for ambenonium and $t_{\frac{1}{2}} = 50$ min for dimethylcarbamylating agents (pyridostigmine and neostigmine) at the same temperature. This may explain prolonged pharmacological response (Konstantin A. Petrov, Irina V. Zueva, Vladimir V. Zobov, Evgeny E. Nikolsky and Patrick Masson, unpublished work). Slow pharmacokinetics [the pharmacokinetics of C-547 injected into the rat is slow, with a half-life in the bloodstream of ∼6 h (Konstantin A. Petrov, Irina V. Zueva, Vladimir V. Zobov, Evgeny E. Nikolsky and Patrick Masson, unpublished work)] also probably contribute to prolonged efficacy in the body. However, at that point, we cannot exclude the possibility that C-547 binds to other targets and may induce unwanted side effects. Thus study of other 6-methyluracil derivatives is in progress aiming at increasing selectivity for the AChE target, increasing the AChE-residence time, and accelerating the pharmacokinetics in the bloodstream for sustained pharmacological effects with reduced side effects.

AUTHOR CONTRIBUTION

Vladimir S. Reznik and Vladimir V. Zobov synthesized the C-547 compound. Alexandra D. Kharlamova, Irina V. Zueva and Eric Krejci performed biochemical experiments (enzyme titration and kinetic measurements). Florian Nachon and Marielle Villard-Wandhammer expressed and purified recombinant AChEs, and determined the 3D structure of the mAChE–C-547 complex. Ekaterina D. Kots performed MD simulations. Sofya V. Lushchekina, designed, performed and analysed MD simulations and molecular modelling on mAChE and hAChE, and wrote the corresponding parts of the paper. Konstantin A. Petrov and Evgeny E. Nikolsky designed the biochemical experiments. Patrick Masson purified human plasma BChE, designed and analysed kinetic data and wrote the paper.

ACKNOWLEDGEMENTS

We are grateful to the M.V. Lomonosov State University Research Super Computer Center and to the Kazan Department of the Joint Supercomputer Center of the Russian Academy of Sciences Branch of Federal State Institution Scientific Research Institute for System Analysis of the Russian Academy of Sciences for providing Lomonosov super computer time.

FUNDING

The molecular modelling part of the study was supported by the Russian Foundation for Basic Research (RFBR) [grant number 13-00-40286-K (to E.D.K. and S.V.L.)]. The experimental part of the study was supported by the Russian Scientific Foundation [grant number 14-50-00014 (to A.D.K., K.A.P., I.V.Z., V.S.R., V.V.Z. and E.E.N.)].

REFERENCES

1 Patrick, J. and Lindstrom, J. (1973) Autoimmune response to acetylcholine receptor. Science **180**, 871–872 CrossRef PubMed

2 Fambrough, D.M., Drachman, D.B. and Satyamurti, S. (1973) Neuromuscular junction in myasthenia gravis: decreased acetylcholine receptors. Science **182**, 293–295 CrossRef PubMed

3 Berrih-Aknin, S. and Le Panse, R. (2014) Myasthenia gravis: a comprehensive review of immune dysregulation and etiological mechanisms. J. Autoimmun. **52**, 90–100 CrossRef PubMed

4 Mehndiratta, M.M., Pandey, S. and Kuntzer, T. (2014) Acetylcholinesterase inhibitor treatment for myasthenia gravis. Cochrane Database Syst. Rev. **10**, CD006986 PubMed

5 Mantegazza, R., Bonanno, S., Camera, G. and Antozzi, C. (2011) Current and emerging therapies for the treatment of myasthenia gravis. Neuropsychiatr. Dis. Treat. **7**, 151–160 CrossRef PubMed

6 Davis, R. (1967) Electron microscopic localization of acetylcholinesterase and nonspecific cholinesterase at the neuromuscular junction by the gold-thiocholine and gold-thiolacetic acid methods. J. Cell Biol. **34**, 157–171 CrossRef PubMed

7 Petrov, K.A., Girard, E., Nikitashina, A.D., Colasante, C., Bernard, V., Nurullin, L., Leroy, J., Samigullin, D., Colak, O. and Nikolsky, E. (2014) Schwann cells sense and control acetylcholine spillover at the neuromuscular junction by α_7 nicotinic receptors and butyrylcholinesterase. J. Neurosci. **34**, 11870–11883 CrossRef PubMed

8 Leader, H., Wolfe, A.D., Chiang, P.K. and Gordon, R.K. (2002) Pyridophens: binary pyridostigmine – apraphen prodrugs with differential inhibition of acetylcholinesterase, butyrylcholinesterase, and muscarinic receptors. J. Med. Chem. **45**, 902–910 CrossRef PubMed

9 Eckert, S., Eyer, P., Muckter, H. and Worek, F. (2006) Kinetic analysis of the protection afforded by reversible inhibitors against irreversible inhibition of acetylcholinesterase by highly toxic organophosphorus compounds. Biochem. Pharmacol. **72**, 344–357 CrossRef PubMed

10 Herkert, N.M., Thiermann, H. and Worek, F. (2011) In vitro kinetic interactions of pyridostigmine, physostigmine and soman with erythrocyte and muscle acetylcholinesterase from different species. Toxicol. Lett. **206**, 41–46 CrossRef PubMed

11 Dawson, R.M. and Poretski, M. (1985) Carbamylated acetylcholinesterase: acceleration of decarbamylation by bispyridinium oximes. Biochem. Pharmacol. **34**, 4337–4340 CrossRef PubMed

12 Yamamoto, K., Sawada, Y. and Iga, T. (1995) Comparative pharmacokinetics of four cholinesterase inhibitors in rats. Biol. Pharm. Bull. **18**, 1292–1295 CrossRef PubMed

13 Kumar, V. and Kaminski, H.J. (2011) Treatment of myasthenia gravis. Curr. Neurol. Neurosci. Rep. **11**, 89–96 CrossRef PubMed

14 Hodge, A.S., Humphrey, D.R. and Rosenberry, T.L. (1992) Ambenonium is a rapidly reversible noncovalent inhibitor of acetylcholinesterase, with one of the highest known affinities. Mol. Pharmacol. **41**, 937–942 PubMed

15 Anikienko, K.A., Bychikhin, E.A., Reznik, V.S., Akamsin, D. and Galyametdinova, I.V. (2008) Compounds with the dioxopyrimidine cycle inhibit cholinesterases from different groups of animals. Chem. Biol. Interact. **175**, 286–292 CrossRef PubMed

16 Semenov, V.E., Giniyatullin, R.K., Lushchekina, S.V., Kots, E.D., Petrov, K.A., Nikitashina, A.D., Minnekhanova, O.A., Zobov, V.V., Nikolsky, E.E., Masson, P. and Reznik, V.S. (2014) Macrocyclic derivatives of 6-methyluracil as ligands of the peripheral anionic site of acetylcholinesterase. MedChemComm **5**, 1729–1735 CrossRef

17 Carletti, E., Li, H., Li, B., Ekstrom, F., Nicolet, Y., Loiodice, M., Gillon, E., Froment, M.T., Lockridge, O., Schopfer, L.M. et al. (2008) Aging of cholinesterases phosphylated by tabun proceeds through O-dealkylation. J. Am. Chem. Soc. **130**, 16011–16020 CrossRef PubMed

18 Lockridge, O., Schopfer, L.M., Winger, G. and Woods, J.H. (2005) Large scale purification of butyrylcholinesterase from human plasma suitable for injection into monkeys; a potential new therapeutic for protection against cocaine and nerve agent toxicity. J. Med. Chem. Biol. Radiol. Def. **3**, nihms5095 PubMed

19 Reznik, V.S., Anikienko, K.A., Kurochkin, V.K., Akamsin, V.D., Galyametdinova, I.V. and Bychikhin, E.A. (1998) New class cholinesterase inhibitors: tetralkylammonium derivatives of 6-methyluracil and alloxazine. Dokl. Chem. **362**, 161–163

20 Leuzinger, W. (1971) The number of catalytic sites in acetylcholinesterase. Biochem. J. **123**, 139–141 CrossRef PubMed

21 Ellman, G.L., Courtney, K.D., Andres, V. and Feather-Stone, R.M. (1961) A new and rapid colorimetric determination of acetylcholinesterase activity. Biochem. Pharmacol. **7**, 88–95 CrossRef PubMed

22 Cornish-Bowden, A. (1974) A simple graphical method for determining the inhibition constants of mixed, uncompetitive and non-competitive inhibitors. Biochem. J. **137**, 143–144 CrossRef PubMed

23 Morrison, J.F. and Stone, S.R. (1985) Approaches to the study and analysis of the inhibition of enzymes by slow- and tight-binding inhibitors. Comments Mol. Cell. Biophys. **2**, 347–368

24 Copeland, R.A. (2013) Evaluation of Enzyme Inhibitors in Drug Discovery: a Guide for Medicinal Chemists and Pharmacologists, John Wiley & Sons, Hoboken CrossRef

25 Masson, P. and Lushchekina, S. (2016) Slow-binding inhibition of cholinesterases, pharmacological and toxicological relevance. Arch. Biochem. Biophys. **593**, 60–68 CrossRef PubMed

26 Bevington, P.R. (1969) Propagation of errors. In Data Reduction and Error Analysis for the Physical Sciences, pp. 57–65, McGraw-Hill, New York

27 Ronco, C., Carletti, E., Colletier, J.-P., Weik, M., Nachon, F., Jean, L. and Renard, P.-Y. (2012) Huprine derivatives as sub-nanomolar human acetylcholinesterase inhibitors: from rational design to validation by X-ray crystallography. ChemMedChem **7**, 400–405 CrossRef PubMed

28 Kabsch, W. (2010) XDS. Acta Crystallogr. D Biol. Crystallogr. **66**, 125–132 CrossRef PubMed

29 Vagin, A. and Teplyakov, A. (1997) MOLREP: an automated program for molecular replacement. J. Appl. Crystallogr. **30**, 1022–1025 CrossRef

30 Emsley, P., Lohkamp, B., Scott, W.G. and Cowtan, K. (2010) Features and development of Coot. Acta Crystallogr. D Biol. Crystallogr. **66**, 486–501 CrossRef PubMed

31 Adams, P.D., Afonine, P.V., Bunkoczi, G., Chen, V.B., Davis, I.W., Echols, N., Headd, J.J., Hung, L.W., Kapral, G.J., Grosse-Kunstleve, R.W. et al. (2010) PHENIX: a comprehensive Python-based system for macromolecular structure solution. Acta Crystallogr. D Biol. Crystallogr. **66**, 213–221 CrossRef PubMed

32 Afonine, P.V., Moriarty, N.W., Mustyakimov, M., Sobolev, O.V., Terwilliger, T.C., Turk, D., Urzhumtsev, A. and Adams, P.D. (2015) FEM: feature-enhanced map. Acta Crystallogr. D Biol. Crystallogr. **71**, 646–666 CrossRef PubMed

33 Cheung, J., Gary, E.N., Shiomi, K. and Rosenberry, T.L. (2013) Structures of human acetylcholinesterase bound to dihydrotanshinone I and territrem B show peripheral site flexibility. ACS Med. Chem. Lett. **4**, 1091–1096 CrossRef PubMed

34 Nachon, F., Carletti, E., Ronco, C., Trovaslet, M., Nicolet, Y., Jean, L. and Renard, P.Y. (2013) Crystal structures of human cholinesterases in complex with huprine W and tacrine: elements of specificity for anti-Alzheimer's drugs targeting acetyl- and butyryl-cholinesterase. Biochem. J. **453**, 393–399 CrossRef PubMed

35 Word, J.M., Lovell, S.C., Richardson, J.S. and Richardson, D.C. (1999) Asparagine and glutamine: using hydrogen atom contacts in the choice of side-chain amide orientation. J. Mol. Biol. **285**, 1735–1747 CrossRef PubMed

36 Masson, P., Lushchekina, S., Schopfer, L.M. and Lockridge, O. (2013) Effects of viscosity and osmotic stress on the reaction of human butyrylcholinesterase with cresyl saligenin phosphate, a toxicant related to the aerotoxic syndrome: kinetic and molecular dynamics studies. Biochem. J. **454**, 387–399 CrossRef PubMed

37 Morris, G.M., Goodsell, D.S., Halliday, R.S., Huey, R., Hart, W.E., Belew, R.K. and Olson, A.J. (1998) Automated docking using a Lamarckian genetic algorithm and an empirical binding free energy function. J. Am. Chem. Soc. **19**, 1639–1662

38 Morris, G.M., Huey, R., Lindstrom, W., Sanner, M.F., Belew, R.K., Goodsell, D.S. and Olson, A.J. (2009) AutoDock4 and AutoDockTools4: automated docking with selective receptor flexibility. J. Comput. Chem. **30**, 2785–2791 CrossRef PubMed

39 O'Boyle, N., Banck, M., James, C., Morley, C., Vandermeersch, T. and Hutchison, G. (2011) Open Babel: an open chemical toolbox. J. Cheminform. **3**, 33 CrossRef PubMed

40 Phillips, J.C., Braun, R., Wang, W., Gumbart, J., Tajkhorshid, E., Villa, E., Chipot, C., Skeel, R.D., Kalé, L. and Schulten, K. (2005) Scalable molecular dynamics with NAMD. J. Comput. Chem. **26**, 1781–1802 CrossRef PubMed

41 Best, R.B., Zhu, X., Shim, J., Lopes, P.E.M., Mittal, J., Feig, M. and MacKerell, A.D. (2012) Optimization of the additive CHARMM all-atom protein force field targeting improved sampling of the backbone ϕ, ψ and side-chain χ_1 and χ_2 dihedral angles. J. Chem. Theory Comput. **8**, 3257–3273 CrossRef PubMed

42 Sadovnichy, V., Tikhonravov, A., Voevodin, V. and Opanasenko, V. (2013) "Lomonosov": supercomputing at Moscow State University. In Contemporary High Performance Computing: from Petascale toward Exascale (Vetter, J.S., ed.), pp. 283–307, CRC Press, Boca Raton

43 Humphrey, W., Dalke, A. and Schulten, K. (1996) VMD: visual molecular dynamics. J. Mol. Graph. **14**, 33–38 CrossRef PubMed

44 Vanommeslaeghe, K., Hatcher, E., Acharya, C., Kundu, S., Zhong, S., Shim, J., Darian, E., Guvench, O., Lopes, P., Vorobyov, I. and Mackerell, Jr, A.D. (2010) CHARMM general force field: a force field for drug-like molecules compatible with the CHARMM all-atom additive biological force fields. J. Comput. Chem. **31**, 671–690 PubMed

45 Zhu, X., Lopes, P.E.M. and MacKerell, A.D. (2011) Recent developments and applications of the CHARMM force fields. Wiley Interdiscip. Rev. Comput. Mol. Sci. **2**, 167–185 CrossRef PubMed

46 Mayne, C.G., Saam, J., Schulten, K., Tajkhorshid, E. and Gumbart, J.C. (2013) Rapid parameterization of small molecules using the Force Field Toolkit. J. Comput. Chem. **34**, 2757–2770 CrossRef PubMed

47 Kozlikova, B., Sebestova, E., Sustr, V., Brezovsky, J., Strnad, O., Daniel, L., Bednar, D., Pavelka, A., Manak, M., Bezdeka, M. et al. (2014) CAVER Analyst 1.0: graphic tool for interactive visualization and analysis of tunnels and channels in protein structures. Bioinformatics **30**, 2684–2685 CrossRef PubMed

48 Tummino, P.J. and Copeland, R.A. (2008) Residence time of receptor–ligand complexes and its effect on biological function. Biochemistry **47**, 5481–5492 CrossRef PubMed

49 Xu, Y., Shen, J., Luo, X., Silman, I., Sussman, J.L., Chen, K. and Jiang, H. (2003) How does huperzine A enter and leave the binding gorge of acetylcholinesterase? Steered molecular dynamics simulations. J. Am. Chem. Soc. **125**, 11340–11349 CrossRef PubMed

50 Semenov, V.E., Zueva, I.V., Mukhamedyarov, M.A., Lushchekina, S.V., Kharlamova, A.D., Petukhova, E.O., Mikhailov, A.S., Podyachev, S.N., Saifina, L.F., Petrov, K.A. et al. (2015) 6-methyluracil derivatives as bifunctional acetylcholinesterase inhibitors for the treatment of Alzheimer's disease. ChemMedChem **10**, 1863–1874 CrossRef PubMed

51 Saxena, A., Redman, A.M., Jiang, X., Lockridge, O. and Doctor, B.P. (1997) Differences in active site gorge dimensions of cholinesterases revealed by binding of inhibitors to human butyrylcholinesterase. Biochemistry **36**, 14642–14651 CrossRef PubMed

52 Kaplan, D., Ordentlich, A., Barak, D., Ariel, N., Kronman, C., Velan, B. and Shafferman, A. (2001) Does "butyrylization" of acetylcholinesterase through substitution of the six divergent aromatic amino acids in the active center gorge generate an enzyme mimic of butyrylcholinesterase? Biochemistry **40**, 7433–7445 CrossRef PubMed

53 Harel, M., Sussman, J.L., Krejci, E., Bon, S., Chanal, P., Massoulié, J. and Silman, I. (1992) Conversion of acetylcholinesterase to butyrylcholinesterase: modeling and mutagenesis. Proc. Natl. Acad. Sci. U.S.A. **89**, 10827–10831 CrossRef PubMed

54 Yamamoto, K., Kohda, Y., Sawada, Y. and Iga, T. (1991) Pharmacokinetics of ambenonium, a reversible cholinesterase inhibitor, in rats. Biopharm. Drug Dispos. **12**, 613–625 CrossRef PubMed

Received 16 November 2015/24 February 2016; accepted 26 February 2016
Accepted Manuscript online 29 February 2016, doi:10.1042/BCJ20160084